Delta Force
Permanent Magnet Hall Thruster

AA 322 Final Report

David Dewey, Danny Roberts, Jacob Rork, Avi Soval

William E. Boeing Department of Aeronautics

University of Washington

Seattle WA, 98195-2400

2019-06-07

The core goal of this project lies in evaluating how effectively a simulated magnetic profile can be realized into a physical thruster design. The magnetic field profile for a micro-scale Hall Thruster composed of two Neodymium magnets, a printed PLA channel insulation, and a 95% purity cast iron core of unknown magnetic permeability was designed and optimized using a magnetic modeling software (FEMM). Core goals were minimizing the normal flux density at the channel walls and maintaining a positive magnetic gradient throughout the channel length. The geometry was modeled in CAD and machined per its specifications, and the magnetic profile in the channel of the final thruster was measured using a gaussmeter. Experimental data displayed excellent agreement in satisfying the theoretical considerations, but the unknown permeability of the iron core caused the minimum average % error along the outer channel wall, exit plane, and inner channel wall to be -7.83%, 15.90%, and 64.7%, respectively. For this reason, it is strongly believed that the cast iron core has a permeability far lower than the minimum simulated permeability of 5000 $\frac{H}{m}$. Ultimately, the project validated the simulation capabilities of FEMM and proved that the magnetic profiles produced in it can be effectively and efficiently reproduced in real life.

Nomenclature

B Magnetic Field Strength

J Current Density

I. Introduction

A Hall Thruster is an electromagnetic propulsion engine ideally suited for station-keeping purposes, where it can easily supply the small delta-V required for course corrections at a fraction of the cost, power, and complexity required by analogous chemically powered engines. In the thruster channel, an axial magnetic field with radial symmetry is used to confine and effectively trap a ring of electrons via the J x B force. Neutral gaseous propellant with a high mass and large ratio of second to first ionization energy (such as Xenon) is then diffused into the cylindrical channel, where it is ionized into a plasma by the circulating electrons and accelerated out the exit plane by an electric potential applied between the anode and cathode. The engine derives its name from the Hall current produced by the ring of circulating electrons.

Hall thrusters typically require a few kilowatts of input power to generate anywhere from hundreds of millinewtons to a few Newtons of thrust. Despite this low propulsive power, the high efficiency and extremely small mass consumption of the thrusters makes them ideal for applications in which minor adjustments are required, hence their widespread use in satellite stationkeeping. Additionally, their ability to produce continuous thrust for long periods of time (however small) has made them viable candidates for powering small to mid-sized interplanetary missions, especially when mission time is not a primary constraint.

This project seeks to design and build the magnetic geometry of a micro-scale Hall Thruster, one that could ideally run on no more than an input of 250 W. The propellant injection and anode-cathode circuit are not addressed. Historically, electromagnetic coils have been used to produce the radially symmetric, steady magnetic field. In this experiment, the use of permanent magnets to generate the same field profile will instead be explored. Permanent magnets offer a reduction in cost and complexity compared to their electrical counterparts, and perhaps more importantly, bring down the total power requirements of the thruster [1]. This could significantly reduce the 250 W needed for an equivalent engine. The inability of a permanent setup in modifying the magnetic field to alter the thrust plume does present a drawback, although this is of less concern with the Hall Thruster as it is typically most efficient when running at maximum power and strength. In other words, it is both feasible and desirable to design the optimum magnetic profile, and use the thruster only at 0 or 100% strength in orbit. Thrust vectoring using on-board satellite mechanisms could easily be used to change the direction of acceleration. Thus, the substitution of an electromagnetic circuit with permanent magnets may be a viable design for future Hall Thrusters.

The Finite Element Method Magnetics (FEMM) software was used to design the thruster geometry that would yield the optimal magnetic field profile, and SolidWorks was used to build the 3D model of the thruster. After the thruster components were manufactured, a Gaussmeter and translation stage were used to map the magnetic field profile throughout the thruster. After this, comparisons were made between empirical and theoretical data, allowing for conclusions to be drawn about the potential effectiveness of a micro-scale permanent magnet Hall thruster.

II. Theoretical Considerations

The Hall Thruster is one of the most complicated electromagnetic propulsion devices, in part because its design enables it to take advantage of the Hall Current and simultaneously avoid space-charge limitations. The transversely generated Hall current is typically a major problem in other EM devices, as it promotes unwanted electron mobility and interferes with applied electric and magnetic fields. The Child-Langmuir law on space-charge limitations describes an upper bound on the density of a charge concentration, and heavily constrained the performance of the similar earlier gridded-ion thrusters. Since the accelerating ions in a Hall Thruster actually pull with them an equivalent amount of electrons from the trapped ring, the exit plasma is effectively quasineutral and free from Child's limitations. This allows for great reductions in the physical size of Hall Thrusters, due to the fact that the thruster and its current can be spatially minimized without encountering this ceiling. For the purposes of this experiment, a detailed discussion of the EM and plasma physics governing the motion of the ions and electrons is not necessary, as only the magnetic field is being built.

As of today, there is no closed-form, analytical expression that describes the optimum axial profile of the magnetic field as a function of other constraints, such as exhaust velocity, applied current, propellant mass, or efficiency. Many of these variables can be individually optimized or solved for in terms of others, but there has been comparatively little research done into finding an ideal magnetic profile. This may be due to the fact that other parameters, such as efficiency and exhaust velocity, are more important and solved for first for given mission specifications, leaving the magnetic profile to be generated afterwards accordingly. Additionally, optimizing the profile is a numerically and computationally demanding task, resulting in a thruster that relies more on extensive simulations than analytical approximations. Indeed, a common approach today for designing this field profile is to begin with a guess and then iterate forth towards a more accurate, desirable solution. The following

discussion describes some of the main specifications that guide the optimization and design of the magnetic profile.

Of primary importance in the thruster channel is the limitation of axial electron mobility - electrons drifting towards the anode can cause damage to some of the components and reduce the existing electric potential, negatively impacting the thruster's efficiency and the exhaust velocity of the ions [2]. For this reason, the magnetic profile must have a peak at some point along the channel length - it is in this region of maximum magnetic field strength that the electrons are effectively trapped. This location is known as the exit plane, and is generally designed to coincide with the physical end of the thruster. Making the magnitude of the B field strong enough at the exit plane prevents (to the extent possible) axial electron mobility back towards the anode. Consequently, the magnetic field is designed to be 0 at the anode as well.

However, the magnetic field cannot be too strong at the exit plane, or at any point in the thruster. Charged particles in the presence of a magnetic field experience an azimuthal drift, and the radius of this gyration is known as the Larmor radius. This radius decreases with magnetic field strength, and increases with particle mass. For a Hall thruster to function correctly, the Larmor radius of its two species - ions and electrons - must be carefully calibrated. Specifically, the B field must be weak enough that the ion Larmor radius is significantly longer than the channel scale length; as a result, the ions are accelerated directly out of the thruster without experiencing a rotation or deflection inside it [3]. Conversely, the B field must be strong enough that the electron Larmor radius is small compared to the scale length, as the electron motion will then be dominated by its azimuthal rotation as opposed to any axial drift. Careful selection of the B field to satisfy both these parameters will allow for the successful confinement of electrons and acceleration of ions.

In addition to the magnitude, consideration must also be given to the gradient of the magnetic field. A negative magnetic gradient, for example a field of maximum strength at the anode that decreases along the scale length L, increases the probability of perturbations in the plasma known as plasma instabilities. This can be imagined as moving from a highly constrained region, for example one with a small Larmor radius, to a weaker region with a larger radius that makes it more likely for ions to spiral away in random directions. To prevent this, the field must be designed with a positive gradient along the channel length. As a result, the magnetic field will grow stronger with length, allowing it to funnel and pinch the plasma as required while minimizing random perturbations [4].

As a final design consideration, the magnetic flux normal to the channel walls, especially at the exit plane, must be minimized. During thruster operation, these incident flux lines will cause plasma to bombard the channel walls, causing significant damage to the thruster via erosion and ablation. It is difficult to machine magnets such that their field lines curve around the channel walls and exit, but a much easier alternative is to just modify the geometry of the channel walls. Since the dielectric insulation on the walls has a minimal impact on the electric or magnetic field profiles, the edges of the thruster can simply be tapered or curved such that the field lines flow around them. This is implemented in the design of the thruster [5].

Fig. 1 shows the optimal magnetic field profile graphically for reference.

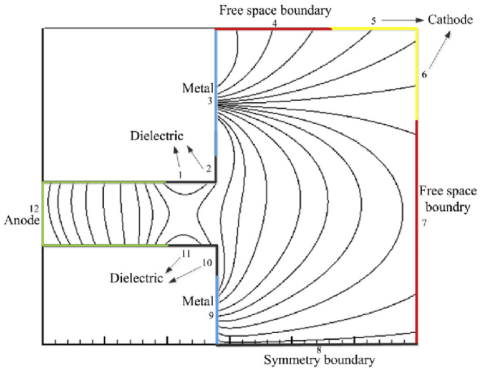

Fig. 1: Ideal Magnetic Field Profile of a Hall Thruster

III. Experimental Apparatus

Neoydimium magnets (NdFeb) are a type of rare earth permanent magnet The dimensions of the permanent magnets and cast iron stock that together make up the magnetic circuit are listed below in Table 1. PLA filament served as a substitute for a dielectric insulator that would be used on a typical Hall Thruster. The specific machine shop tools needed are listed as well. Gaussmeter probes were mounted using a fine-tuning translation stage augmented with an aluminum plate. A 3D printed stand fixed the base of the translation stage and the magnetic circuit together at a distance and angle useful for measuring. Gaussmeter probes were mounted on the plate such that the magnetic field profile in and around the channel could be easily characterized. This apparatus was constructed with the goal of measuring specifically the magnetic field along vertical cross-sections of the thruster as they are particular areas of interest, and so that comparisons between empirical data and FEMM simulations could be easily made.

The translation stage allows for one inch of motion in the X, Y, and Z direction with notches signifying every thousandths of an inch which allows for very accurate displacement control. Meanwhile, the gaussmeter measured to an accuracy of ± 1 Gauss.

The iron core for the thruster contained two pieces that were machined in the Bossart Machine Shop, while the 3D printing and gaussmeter testing took place in the S.P.A.C.E Lab in AERB 013.

Table 1: Used Equipment and Materials

Name	**Notes**
Cast-Iron Rod	D = 4" , L = 12" ASTM A247 Specification
Aluminum Plate	Extension of Translation Stage, used for mounting probes
Inner NdFeB Magnet	OD = 1.498", ID = 1.065", thickness = 0.375", Grade N45
Outer NdFeB Magnet	OD = 3.595", ID = 3.003", thickness = 0.075", Grade N40
Translation Stage	Assist Magnetic Field Characterization
Gaußmeter	Magnetic Field Measurement Device
Gaußmeter Probe (x2, Axial, Normal)	Magnetic Field Measurement Device
3D Printer	LulzBot TAZ 5
PLA 3D Printer Filament	Used to brace the magnetic components
Bossart Machine Shop Tools	Lathe, Band Saw, Mill

IV. Design Procedure

Using the finite element magnetic modeling tool FEMM 4.2, a design for the scale hall thruster was drafted and properties of the magnetic field including the strength and the flux through contours across the bottom and top of the thruster channel as well as the contour parallel to the inner channel wall. The cross-sectional design and magnetic field contour lines generated by the simulations using one NdFeB grade 45 magnet and one NdFeB 40 magnet mounted on an iron core are shown below in Fig. 2. It should be noted that the FEMM software does not allow for the axes or geometric values to be shown on their figures. The figure below is a cross section with X in the radial direction and Y as the vertical direction, with values for the geometries of the core, PLA, and magnets shown below in Figs. 18, 19, 14, and 15, respectively. In the simulation, the regions of vacuum act as a medium with a relative permeability of 1, which allows the magnetic field to exist but does not impact the field in any way. In a standard hall thruster, a dielectric material must be added to

the channel to protect the channel walls, and in the simulations that material was modeled by borosil. Borosil has a relative permeability of .999984, so like the vacuum, it does not significantly impact the magnetic field profile or strength, which ensures that the magnetic field is determined completely by the geometry and relative permeability of the iron core and the strength and geometry of the magnets. In practice, borosil is not a simple material to work with so a 3D printed PLA structure was designed to replace the borosil in the scale thruster, the drawing of which is shown below in Fig. 19. The relative permeability of PLA is also nearly 1 at around .999974 [6], so it acts analogously to borosil in the channel, allowing for accurate comparison between the real measurements and those ran in simulations.

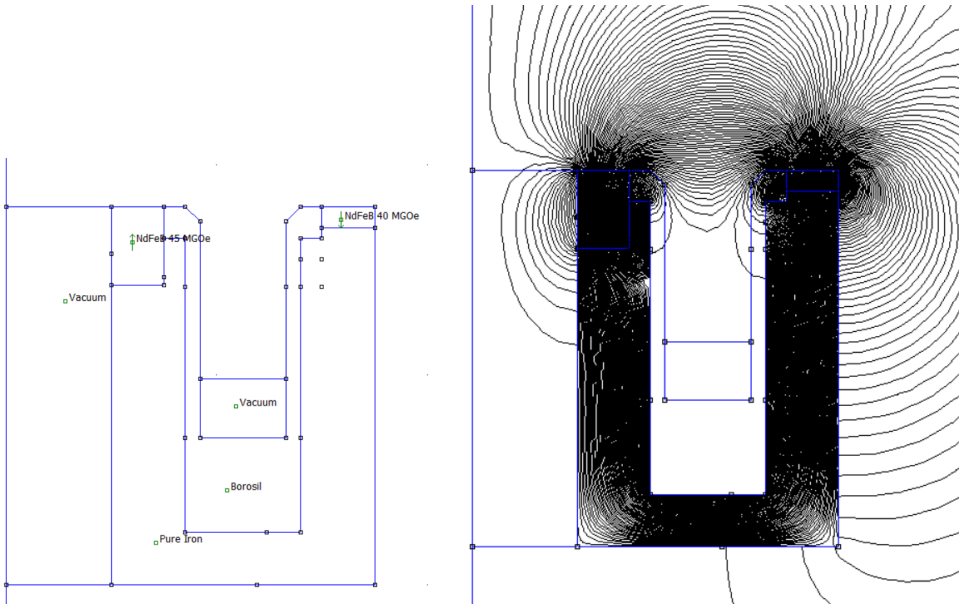

(a) **(b)**

Fig. 2: (a) Simulated and constructed cross section of scale Hall Thruster (b) Magnetic Field lines using acquired magnets

Once the ordered magnets and cast iron arrived, the core was machined in the Bossart Machine Shop. Initially, a single-piece core was to be machined from the cast iron stock, but it was deemed too difficult for the time allotted to machine the channel of the core. Thus, two pieces were made. The first piece was the 'inner core' that consists of the channel floor, interior wall, and slot for the inner magnet to sit in the center of the piece, concentric with the exterior. The second piece was essentially a large ring that sat the outer magnet and makes up the exterior wall of the channel and exterior wall of the thruster. These parts were made using a band saw and lathe, and carefully combined into a single piece using a press fit on a vice. An estimated 30 hours was spent machining the iron core to an accuracy of

$\pm$ 0.003 in for each dimension. Once the magnets were ordered the final budget sheet was updated and is shown in the Appendix in Fig. 21.

For the magnetic field measurements, a gaussmeter was chosen to record the magnetic flux density in and around the channel. The gaussmeter was delivered to the SPACE laboratory and verified to be functional. To get an accurate mapping of the magnetic field profile strength from the gaussmeter probes, a mostly-uniform distribution of steady measurements was taken. To eliminate the human error from manually holding the gaussmeter probes in desired locations, the idea to mount the thruster onto a translation station in which the thruster can be translated in the x, y, and z directions and keep the probes stationary through a separate mounting system was explored and two main problems needed to be solved. First, the probed needed to be elevated up and into the channel while still being able to use the translation stage for incremental movements. To allow for this, 4 1/4 - 20 bolt holes were drilled in an aluminum plate at positions to allow the sheet to be mounted vertically on the stage as shown in Fig 3. A single hole was drilled in the center of the sheet 6" from the base of the translation stage and a flange originally mounted to the stage was bolted to the sheet so the probe could be fed through and down into the channel. The hole on the flange however was larger than the diameter of the gaussmeter probes so any small movement of the stage would shift the tip of the probe significantly causing the positional readings to be inaccurate. To counteract this, a second hole was drilled into the center of the aluminum sheet 5.8" below the original hole and a second flange was mounted so the probe would be fed through not one hole but two holes far apart to keep it steady in the channel. A 3-D printed flange sleeve with two holes, one with the exact diameter of the perpendicular probe and one for the axial probe as shown below in Fig. 17, was designed and printed to slide over the flange to increase positional accuracy even further.

The second problem was holding the translation stage and the hall thruster in the same locations throughout the length of the testing. The solution came through designing a 3-D printed PLA base that had two .3" deep depressions, one with the exact area of the base of the translation stage and one with the exact area of the hall thruster base, which the hall thruster and the translation stage slipped into exactly. lowering positional inaccuracy greatly. This completed the test stage setup which is shown below in Fig. 3. Once the testing stage was complete, the experiment was ready to begin.

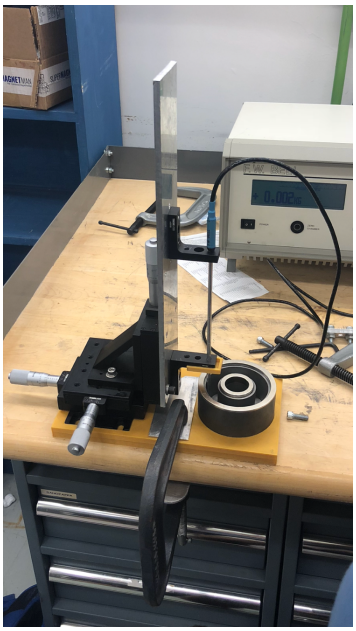

Fig. 3: Completed Test Stage including 3-D printed base and flange sleeve, and aluminum sheet

V. Testing Procedure

Testing was completed using both a perpendicular magnetic field probe as well as an axial magnetic field probe tested one after the other. This was to map not only an accurate magnitude using superposition, but also direction of the field inside the channel from the inverse tangent of the axial over the perpendicular readings. Starting with the perpendicular probe, the probe was fed through the two flanges of the testing stage and was lowered to .25" above the channel base and placed up against the inner wall. Then, the translation stage was used to move the probe from the inner to the outer channel wall which was defined as the X direction, at which 8 magnetic field strength readings were taken at equal distances apart. The channel width is .554" so measurements were taken at about .07" distances, which is easily achievable using the translation stage. Once the 8 measurements horizontally were taken, the probe was elevated in the Y direction and then 8 more horizontal readings going from the outer channel wall to the inner channel wall were recorded. This snaking patterned from inner to outer then outer to inner channel wall continued until the entire channel was mapped in the X and Y direction. The vertical measurements were taken from .27" to 1.52" was divided into 26 vertical points spaced equally at .048", creating a full 8 by 26 grid of values of the magnetic field strength. While the channel height is only 1.4", the magnetic field behavior just above the channel was desired along with the strength properties in the channel. The values were recorded visually at each and transferred into an excel spreadsheet.

Once the perpendicular measurements were recorded, the axial probe was fed through the two flanges of the test stage and centered at the inner channel wall .25" from the base and the above steps were repeated until an 8 by 26 grid of axial measurements was recorded. After a single plane was mapped in both the perpendicular and axial direction, the data was ready for analysis. The final gantt chart used to map the tasks for the experiment is shown below in Fig. 20.

VI. Results and Discussion

FEMM and Design Results

Using FEMM to test multiple designs, the iron core geometry that produced a magnetic field profile most consistent with the parameters listed in the theory section was found. The core has a base thickness of .25 in., outer and inner channel wall thickness of .35 in. , with a left and right flange height from the base to the magnet of 1.42 in. and 1.7 in., respectively. The simulation was conducted using the N45 and N40 magnets purchased for the project as well as the desired iron geometry stated above. As shown below in Fig. 4, the generated magnetic field profile is almost fully symmetric about the center of the channel with just slight differences in the magnetic field on either side of the center of the channel. This, visually, is as ideal of a magnetic field profile expected for the project given the limitation to use only magnets available online and is verified through the Hall Thruster theory. The magnetic flux through the inner channel wall and the flux across the center of the channel where the vacuum region meets the PLA are shown below in Fig. 5. The vertical red line, measured from bottom to top, is where the normal inner wall flux was measured while the horizontal red line across the channel is where the normal channel flux was measured. As shown in Fig. 5a, the normal flux through the inner wall remains zero for most of the length which is ideal. There is a slight bump in the flux then a large decrease near the top of the channel, which is due to the proximity of the iron to the magnet near the top of the channel, which causes the field to loop back onto the channel wall. But even after the bump and drop off the flux through the wall never gets above a .08[B] magnitude. Fig. 5b shows that the flux normal to the center of the channel inside the channel is very small across the entire length, with a maximum magnitude of 7×10^{-5} [B] recorded around 62.5% of the distance from left to right, which is what was expected from the hall thruster theory with permanent magnets.

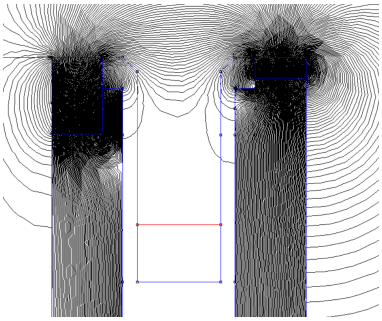

Fig. 4: Symmetric Magnetic Field Profile and lines of location of normal flux measurements

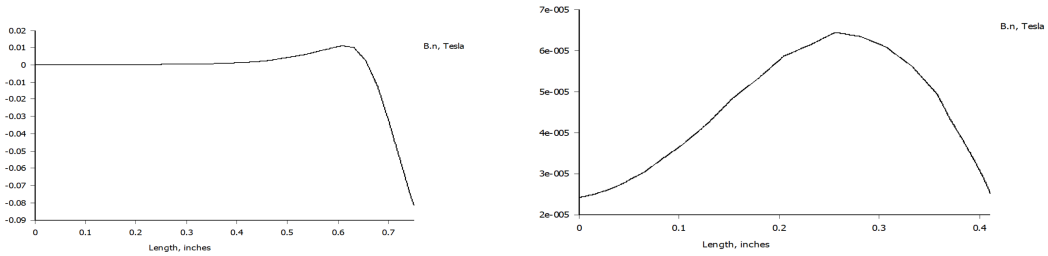

(a) **(b)**

Fig. 5: (a) Final Design Magnetic Flux normal to the inner channel wall (measured in Tesla) (b) Magnetic Flux across the center of the channel at the PLA (measured in Tesla)

The above results were taken again from the final design for the Hall Thruster using the purchased NdFeb magnets. For reference, the magnetic solution for the flux through the same boundaries as above for the optimal case where both the magnet geometry and iron geometry can be altered without restriction is shown below in Fig. 6. For both the flux through the inner channel wall and the through the center of the channel, the shape of the flux profile is nearly identical to that of the purchased magnet design. The values however for the optimal case are much smaller as presented in Table 2, but that can be attributed to the increase in strength of the magnets used for the original simulation versus the final simulation, as the original simulation used two 32 Grade NdFeb magnets while the the final design uses one 40 grade and one 45 grade magnet. The uncertainty values were calculated using a triangular error pdf. Ideally, the optimal design would be pursued, but again due to the limitations of machining neodymium along with the limited shapes and grades available through online vendors, the slightly larger flux values had to work for the experiment. In reality, this increased flux through the channel wall would lower the life span of the thruster due to the breakdown of the channel wall, but for the design and verification of the magnetic field for the small scale thruster this was tolerable.

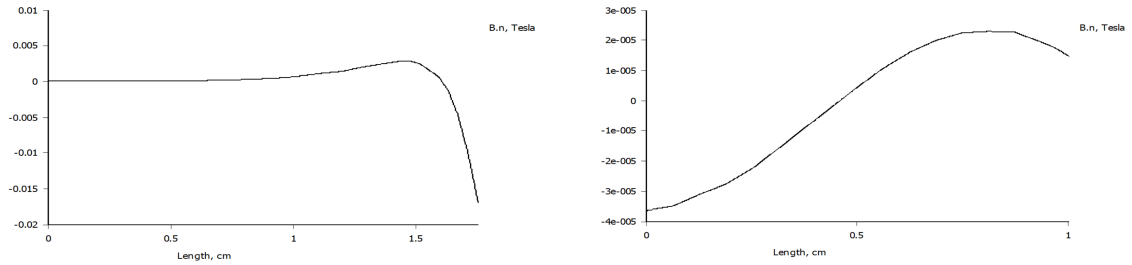

(a) **(b)**

Fig. 6: (a) Ideal Magnetic Flux Normal to Inner Channel Wall [B] (b) Magnetic Flux across the Channel Center at PLA Boundary [B]

Table 2: Flux Comparison for Optimal vs. Final Design

Design	**Channel Max[B]**	**Inner Wall Flux Bump[B]**	**Inner Wall Flux Min.[B]**
Optimal Design	2.4×10^{-5}	$.0045 \pm .0005$	$-.015 \pm .005$
Final Design	6.5×10^{-5}	$.012 \pm .008$	$-.08 \pm .008$

The FEMM results for the final thruster design including the values presented in the table above are what will be used for the final verification of the magnetic field to ensure the simulated magnetic field profile is what will be generated for the design in the laboratory setting.

Experimental Results - Comparing to Design Theory

The following section analyzes the final experimental data collected for the experiment and compares it to simulated FEMM data for a range of magnetic permeabilities. The final test section data was stored in a 26 x 8 matrix, representing measurements taken at 26 heights vertically up the channel of the thruster and 8 radial positions across it. From the experimental normal and tangential data, a magnitude matrix was generated as well as an associated vector plot showing the actual field lines throughout the thruster. As required by the theoretical design considerations, the magnetic flux throughout the channel is minimal until it drastically starts to increase near the exit plane. For this reason, contour plots for both the entire test section and the exit plane region are given, to provide flux information for the entire channel as well as a more descriptive illustration of its exit. The test section and exit plane graphs for total, normal, and tangential magnetic field magnitudes are shown below in Fig. 7 (a) - (f), respectively.

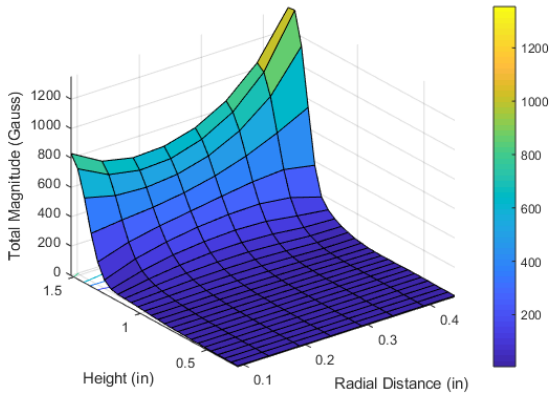

(a) Net Mag, Full Test Section

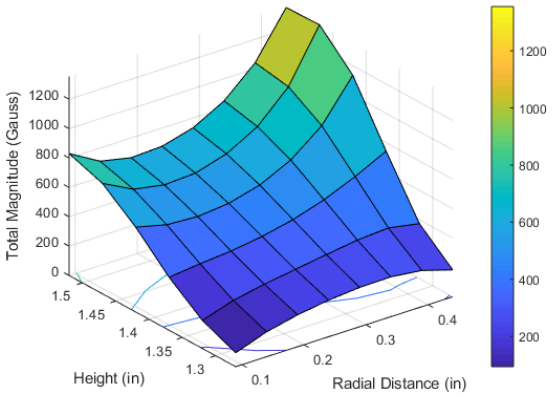

(b) Net Mag, Exit Plane

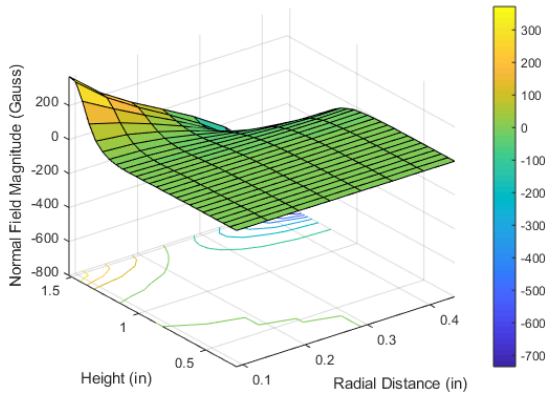

(c) Normal Mag, Full Test Section

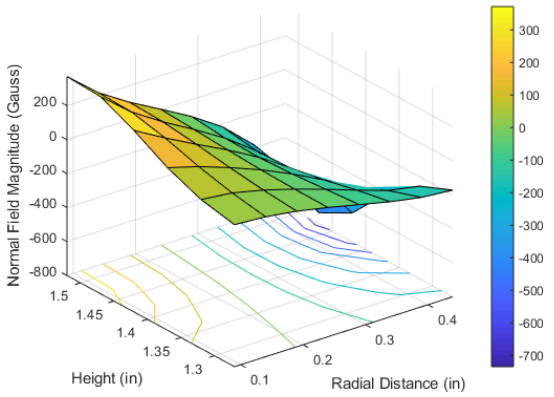

(d) Normal Mag, Exit Plane

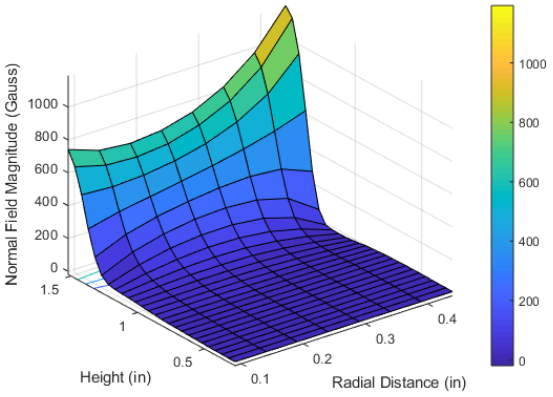

(e) Tang. Mag, Full Test Section

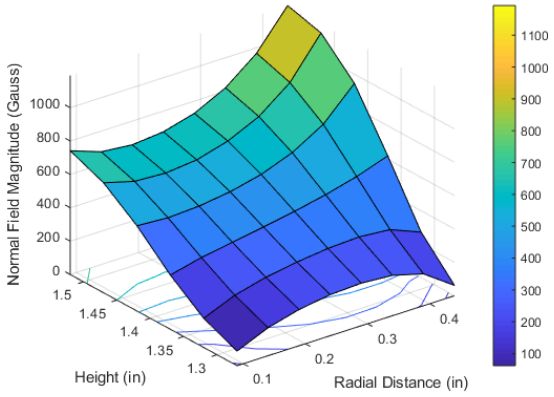

(f) Tang. Mag, Exit Plane

Fig. 7: Total, Normal, and Tangential Magnetic Field Magnitudes (Gauss)

In these graphs, the X-axis measures the radial distance in inches from the outer edge of the channel wall, so moving along the X-axis is equivalent to moving towards the center of the thruster. The Y-axis measures the height in inches from the bottom of the thruster channel, and the Z-axis plots the field magnitude in Gauss.

During the design process as guided by the theoretical considerations, the three primary goals were: to have a B field profile that rises from 0 at the anode to a peak at the exit plane, to ensure the B field gradient is smooth and positive along the channel length (corresponding to height), and to minimize the magnetic flux normal to the channel walls. Here, the channel wall refers to the PLA wall, which would take the place of dielectric shielding in a functioning thruster. The graphs above are well suited to evaluate the first two of these objectives. It is clear from Figs. 7a, 7c, and 7e, and from the exact measurements, that the magnetic field in the thruster channel remains near 0 until approximately 1.02" above the thruster bottom. Similarly, the same figures demonstrate that that the field magnitudes peak at the exit plane. Figures 7b, 7d, and 7f depict how the gradient of the magnetic field magnitude is continuously positive as height along the channel increases. Even though Fig. 7d shows the tangential field becoming sharply negative, the magnitude has increased, thus still satisfying theoretical expectations. All 6 figures also show the field magnitude at the inner channel exit plane as significantly larger than the magnitude at the outer channel; this matches expectations due to the inner magnet being slightly stronger.

The boundaries of the test section coincide with the walls of the printed PLA insulation. Thus, the first and final columns in the tangential data matrices correspond to the flux normal to the outer and inner channel walls, respectively. The tangential data is used for the this normal flux calculation since the orientation of the axes in the test data is perpendicular to the contours drawn in FEMM. A plot of the normal flux across each of the walls is shown below in Fig. 8

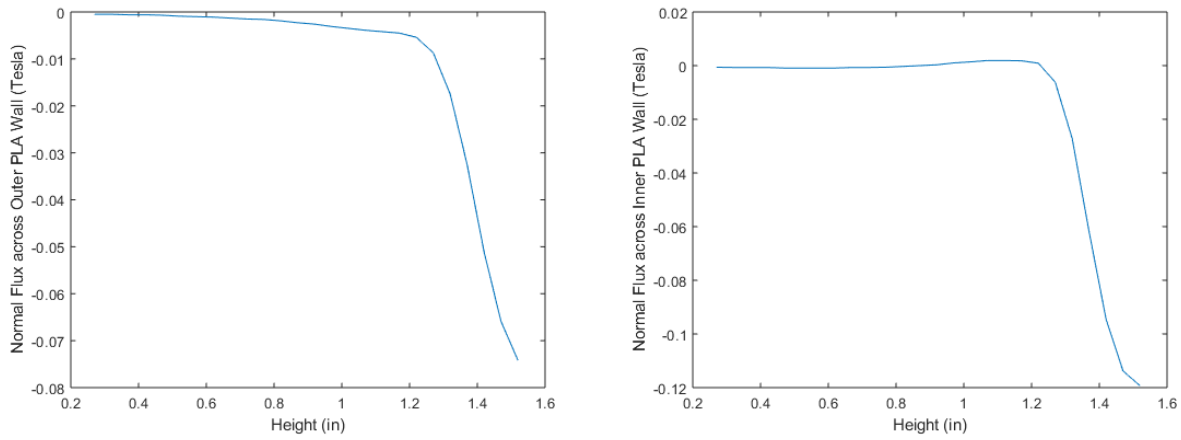

(a) Outer Wall **(b)** Inner Wall

Fig. 8: Normal Flux across Channel Walls (Tesla)

These contours excellently satisfy the theoretical requirements of minimal normal flux and agree strongly with the simulated data from FEMM shown in Fig. 5. The normal flux remains 0 until approximately 1.2" up the channel length, at which point it sharply begins to increase to 0.1 Tesla, or 1000 Gauss. Though these are relatively high fluxes, they are modeled for a contour that continues vertically up the entire channel length, and do not account for the tapered tip of the dielectric. Thus, the normal flux here would actually miss the dielectric, increasing the lifetime of such an insulator even more.

A vector profile showing the orientation and magnitude of the field lines throughout the test section was also produced using the normal and tangential measurements, and is shown below in Fig. 9. This plot seems somewhat empty due to the fact that it is only modeling a small section of the magnetic field profile in the thruster channel instead of the entire field around it, but it still demonstrates well the directionality of the flux and relative strengths of the magnets.

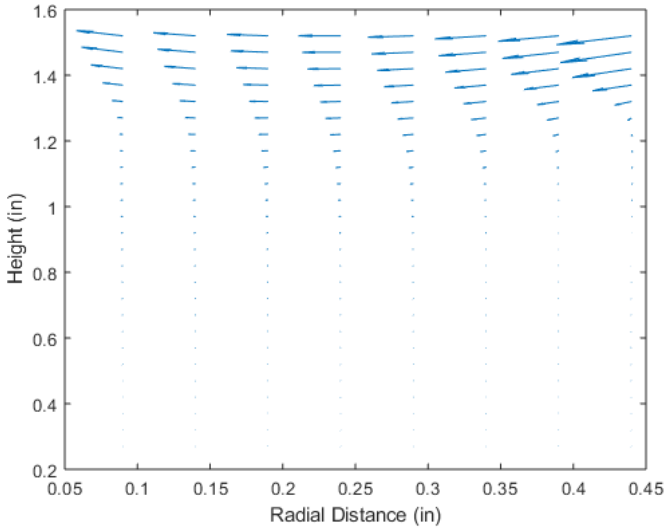

Fig. 9: Magnetic Field Profile

Fig. 9 accurately shows the orientation of the magnetic field, and shows the magnetic field strongest at the channel walls and weaker in the channel center line, as expected.

The adherence of the physical thruster's magnetic field characteristics to theoretical design considerations has now been well established and substantiated. As desired, the magnetic field peaks at the exit plane as it follows a positive gradient along the channel scale length (height). Minimal incident normal flux into the channel walls was also maintained excellently. The following section will now analyze how well the experimental data compare to a set of FEMM simulations that iterate through a range of unknown permeabilities.

Experimental Results - Comparing to FEMM

As stated earlier, one of the overarching unknowns in this project was the magnetic permeability of the impure cast iron used (due to cost contraints). Consequently, one of the major goals over the course of this experiment was to analyze how changing the permeability of the iron impacts the resultant FEMM simulations.

In FEMM, pure iron has a relative magnetic permeability of 14872 $\frac{H}{m}$, which is far beyond the approximately 95% grade cast iron used for the thruster. As carbon is introduced into iron, the metallic lattice becomes impure as carbon atoms form new bonds and disrupt the previously ordered arrangement of the iron. As a result, the material begins to lose its magnetic permeability, and therefore becomes less efficient at guiding field lines. Thus, it is

expected that the use of 95% cast iron in this project will negatively impact the iron core's ability to shape the field lines in the thruster channel. To gauge the effect of permeability, the thruster geometry was simulated in FEMM changing only the iron permeability from 5000 - 14000 in steps of 1000 $\frac{H}{m}$.

For each simulated permeability, full test section and exit plane contours were generated for the total, normal, and tangential field magnitudes as in Fig. 5. It is not easy to visualize the changing surface contours against each permeability iteration, as doing so would require superimposing the 10 color maps for each type of magnitude on each other. Additionally, from a preliminary analysis of the contours in each of the simulations, it is exceptionally difficult to identify significant changes from one permeability to the next, even when focused in on the exit plane. For this reason, instead of analyzing the surface contours of every permeability, the *error* between each simulation and the experimental data was analyzed and organized. Both the absolute error and percentage error were calculated for these comparisons, since theoretical readings for the bottom of the channel were typically a few Gauss, while readings near the exit plane were roughly on the order of 10^3 Gauss, causing percentage errors at the bottom to be orders of magnitude higher than those at the top, even though the actual magnitude of the errors were way smaller.

For each tested permeability, the percentage and absolute errors were computed only as a function of channel height and parameterized by the permeability. That is, each of 26 rows corresponding to a particular channel height were assigned a single value that was the average of either the percentage or absolute error *for that entire* row. This was then iterated over the 10 tested permeabilities, yielding a final 26 x 10 matrix. The systemic errors that may arise from treating the data this way will be addressed in the error analysis section. Since the first inch of the channel wall has negligible field readings, the error graphs focus only on the region around the exit plane. Additionally, only the total magnitude plot is provided, as the primary concern here is finding how permeability changes the total magnetic field.

Fig. 10 below provides a contour plot as well as a 2D projection of the surface for the absolute error between expected and theoretical measurements across the range of simulated permeabilities. Likewise, Fig. 11 does the same except for the percentage error.

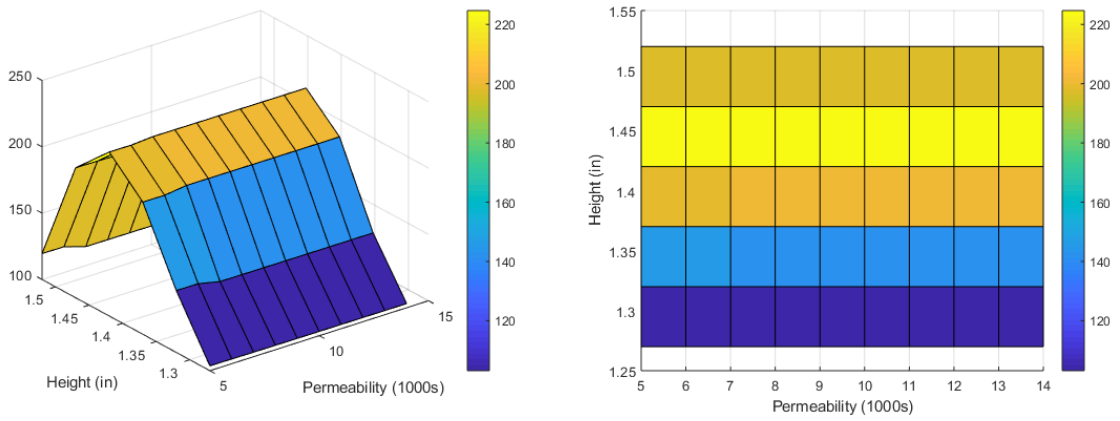

(a) Contour **(b)** 2D Projection

Fig. 10: Absolute Error at Each Height as a Function of Permeability

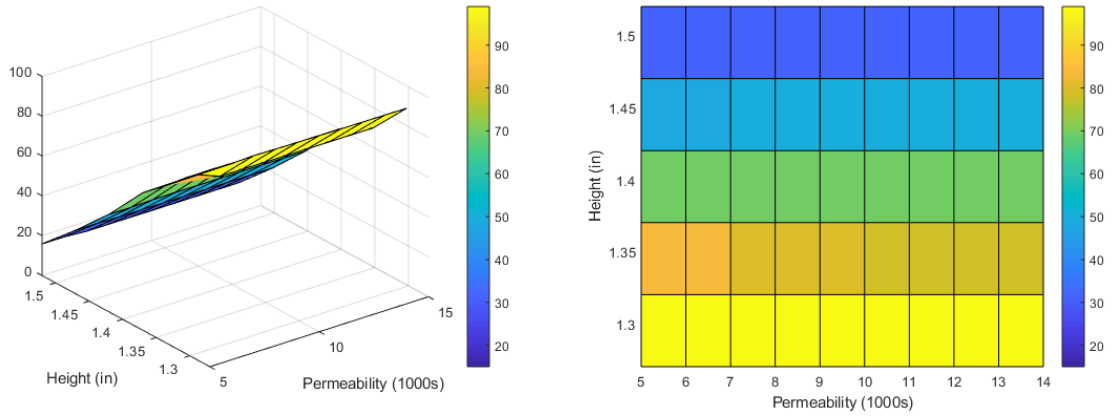

(a) Contour **(b)** 2D Projection

Fig. 11: Percentage Error at Each Height as a Function of Permeability

Analyzing the above figures leads to the conclusion that the error at each height is almost exclusively a function of only the height, and is hardly impacted by changing the permeability. In both Figs. 10b and 11b, it is apparent that each row of error remains essentially constant across the entire permeability. As mentioned earlier, it is expected that the percentage error will drop as height increases, since the magnitude of the measurements will increase - this is demonstrated in Fig. 11b, where % error drops from approximately 90% below the exit plane to less than 25% at it. Likewise, it was expected that the absolute error rise as height increases - this is echoed in Fig. 10b. However, the absolute error curiously

peaks at approximately 1.47" from the channel base, corresponding to a location right above the end the actual iron core but still below the axis that marks the top of the magnets. It is likely that this peak is due to positional uncertainty between the lattices of the experimental data and the simulated test section, and will be discussed more in the error analysis section.

As shown above, the absolute error increases with height while the percentage error decreases, and both remain relatively invariant under permeability changes. However, from Figs. 10a and 11a it is apparent that the magnitudes of these errors decrease slightly with decreasing permeability, suggesting that the cast iron purchased may actually be of a permeability lower than 5000 $\frac{H}{m}$. For a final comparison between the simulated and experimental data, Figs. 12 and 13 below depict the 2D and 3D absolute and percentage errors for the 5000 permeability test, respectively. Since only one permeability is shown here, both figures thus compute these error margins at each individual point in the test lattice, again only in the vicinity of the exit plane. Since this contour is for the lowest simulated permeability, the error margins here should be the lowest out of all the iterated permeabilities.

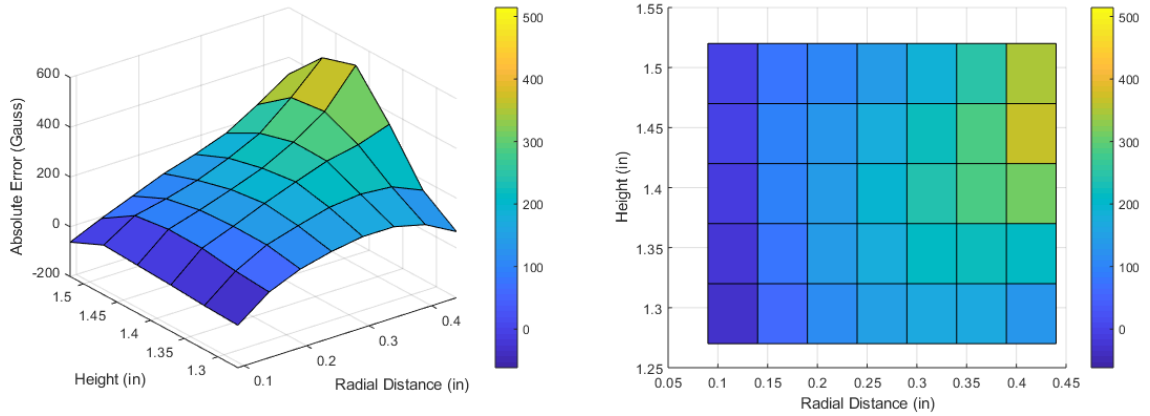

(a) Contour **(b)** 2D Projection

Fig. 12: Absolute Error for Permeability = 5k

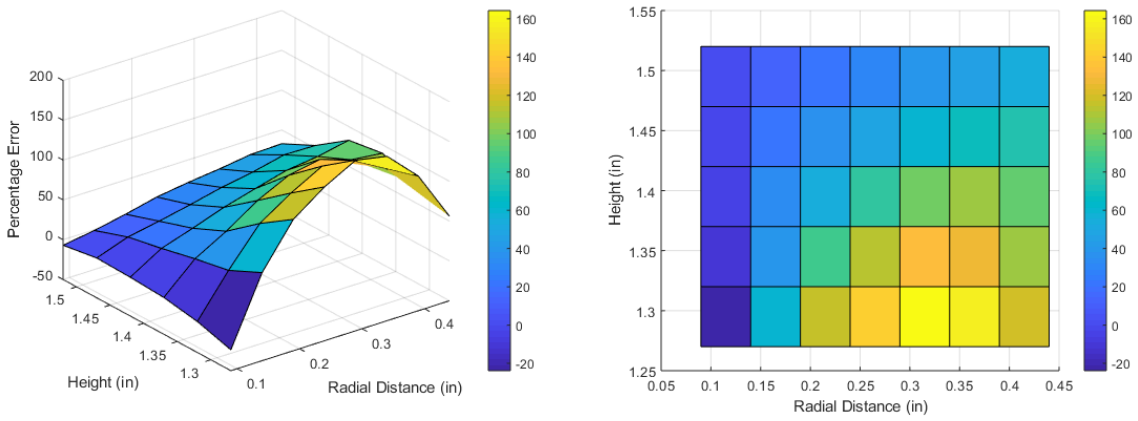

(a) Contour **(b)** 2D Projection

Fig. 13: Percentage Error for Permeability = 5k

Both figures above echo the insights provided by the permeability error contours, namely that the absolute error should increase with height and the percentage error should decrease. However, now due to the fact that only a single test section is being analyzed, it is also possible to see how the error changes with radial distance in from the outer channel wall. Measurements taken at this outer channel wall displayed both the lowest absolute and percentage errors of anywhere in the test matrix, averaging only a -7.83% error that was relatively constant with height. Moving radially across the channel towards the inner wall and near the height of the exit plane had the impact of increasing both percentage and absolute errors, which was to be expected due to the higher strength of the inner magnet. Figure 9a also helps explain why the absolute error contour in Fig. 10a peaked at a specific height for all tested permeabilities - this abrupt jump is actually due to a high absolute error measurement right at the inner channel wall next to the magnet, corresponding to a radial distance of 0.45" and height of 1.47". Since any positional uncertainty effects on magnitude would be magnified so close to the magnet, and since Fig. 10a compounds the error for each row, it is likely that the peak in the absolute error contour is caused by this single high measurement, which in turn heavily weights the average for that row.

The key takeaway from this analysis is that permeability has little impact on the simulated FEMM data for the magnetic field, but that lower permeabilities subtly reduce the error margins between the simulated and experimental data as they more accurately represent the properties of the impure cast iron used for this experiment. At the lowest tested permeability of 5000 $\frac{H}{m}$, percentage errors in the axis of the exit plane averaged 15.90%, while those

along the outer channel wall averaged only -7.83%. Along the inner channel wall, the average percentage error was 64.7%, to highly variable positional uncertainties that will be discussed shortly. Ultimately, given the trends in the permeability contours, it is likely that the cast iron core purchased has a permeability significantly smaller than 5000 $\frac{H}{m}$. The following section will discuss the error inherent in each step of the experiment and examine its impact on the data.

Error Analysis

There were three primary sources of error that impacted the quality of the measurements as well as their comparison to simulations. As discussed earlier, the 26 x 8 matrix of test points corresponds to a lattice ranging from 0.27 - 1.52 inches in height and 0.09 - 0.44 inches in distance from the outer wall. This lattice was defined first in FEMM, and simulations for the field magnitudes were run on contours that spanned the exact position of each point in the lattice. However, this test matrix did not spatially transfer perfectly to the actual measurements made on the thruster, for a few main reasons. In the initial setup for the experiment, the weight of the thruster and translation stage actually compressed the ends of the PLA base and caused the center to arc upwards - causing the translation stage to be inclined backwards by a small degree relative to the thruster. Additionally, the axial and tangential probes were not completely straight. Furthermore, there is the likelihood that the channel itself was not machined exactly to the design of the FEMM geometry. The first of these error sources was mitigated by clamping down the center of the base to remove its arc, but the remaining sources likely compounded to introduce moderate positional uncertainty. This positional uncertainty would increase moving up the height of the test matrix, as any angular inclinations would sum together and cause points higher up to be radially deflected more than points at the bottom of the thruster. However, the error percentage at the exit plane in Fig. 13b decreases with height, so it seems as if this positional uncertainty does not play as large of a role as initially thought.

The permeability graphs for the exit plane region in Figs. 10 and 11 took average error values for each height value, and thus lose any resolution or insight as to how the error changes as a function of radial position. Any conclusions derived from these permeability simulations could be misleading as to the permeability that produces the minimum error, since they misrepresent trends in the error. However, given that the magnitude surface contours across all tested permeabilities had minimal variation, it can be assumed that the exit plane graph for a permeability of 5000 $\frac{H}{m}$ in figure 13b is a good representation of the radial

error variation. This graph, as discussed earlier, shows strong measurement agreement along the outer channel wall, and even along the exit plane. The inner channel error is higher in magnitude than the outer wall, but still trends downwards to lower values. Thus, this error map reaffirms the agreement of the magnetic profile of the thruster with theoretical guidelines, while the permeability error contours in Figs. 10 and 11 strongly suggest that the permeability of the cast iron core is significantly below 5000 $\frac{H}{m}$

VII. Conclusions

FEMM 4.2 was utilized in the preliminary design phase of the project to create an optimal thruster geometry. This geometry was characterized by a minimized normal flux density at the channel walls and a positive magnetic gradient that peaked at the exit plane. Due to cost constraints, the pure iron modeled in FEMM was not available to purchase and a lower quality cast iron of unknown permeability was used. Hence, a significant portion of the data analysis was devoted to simulating field profiles in FEMM over a range of permeabilities and then comparing these to the measured data.

The experimental data satisfied excellently the theoretical design parameters, keeping the normal flux density at roughly 0.01 Tesla until the exit plane, where it peaked to 0.1 Tesla as predicted by FEMM. The magnitude of the field profile for most of the scale length was also 0 as desired, until sharply increasing to its maximal radial distribution at the exit plane, ensuring the thruster's ability to actually pinch and guide a plasma. FEMM simulations suggested that the commercially purchased cast iron had a permeability of far lower than 5000 $\frac{H}{m}$, as even at these lowest error margins the average % error along the outer channel wall, exit plane, and inner channel wall were -7.83%, 15.90%, and 64.7%, respectively. Positional uncertainty hypothetically may have caused error margins to increase through the scale length of the thruster, but analysis of the permeability simulations suggests that this is not the case and that the majority of the error does in fact arise from the unknown permeability of the thruster.

This project has been an excellent foray into the complicated physical theory behind Hall Thrusters, techniques for simulating magnetic profiles, and provided excellent machining and industry expertise. The results match excellently with the theory and the design predicted by FEMM, and resoundingly accomplish the project's ultimate goal of physically and accurately realizing the simulated magnetic profile of a Hall Thruster.

VIII. Acknowledgements

This project was completed with the assistance of:
Professor Justin Little
Professor Jim Hermanson
PHD Research Assistant Peter Thoreau
Senior Research Assistant Reed Thompson
Bossart Machine Shop Shopmaster Dzung Tran
The UW AA Department Fiscal Office

IX. References

[1] Renaudin, P. e. a., *Magnetic Properties of Materials*, The French Laboratory of Magnetics.

[2] Goebel, D., K. I., *Fundamentals of Electric Propulsion: Ion and Hall Thursters*, Jet Propulsion Laboratory, California Institute of Technology, 2008.

[3] Rossi, Alberto, e. a., *Parametric Optimization of a Hall Thruster magnetic circuit*, International Symposium on Space Technology and Science, 2015.

[4] Peterson, P. G. e. a., *Experimental Investigation of the Internal Magnetic Field Topography of an operating Hall Thruster*, Physics of Plasmas, 2002.

[5] Kornberg, O., *Investigation of Magnetic Field Profile Effects in Hall Thrusters*, Embry-Riddle Aeronautical University, 2007.

[6] Strunk, W., *The elements of style*, Penguin, 2007.

X. Appendices

3-D models of each of the four components of the mock-up hall thruster were designed and drawn in Solidworks 2018. The final part drawings are included below in Figures 14, 15, 18, 19. Project timeline and task dependencies are outlined in the Gantt Chart shown in Figure 20. The final project budget is shown in Figure 21.

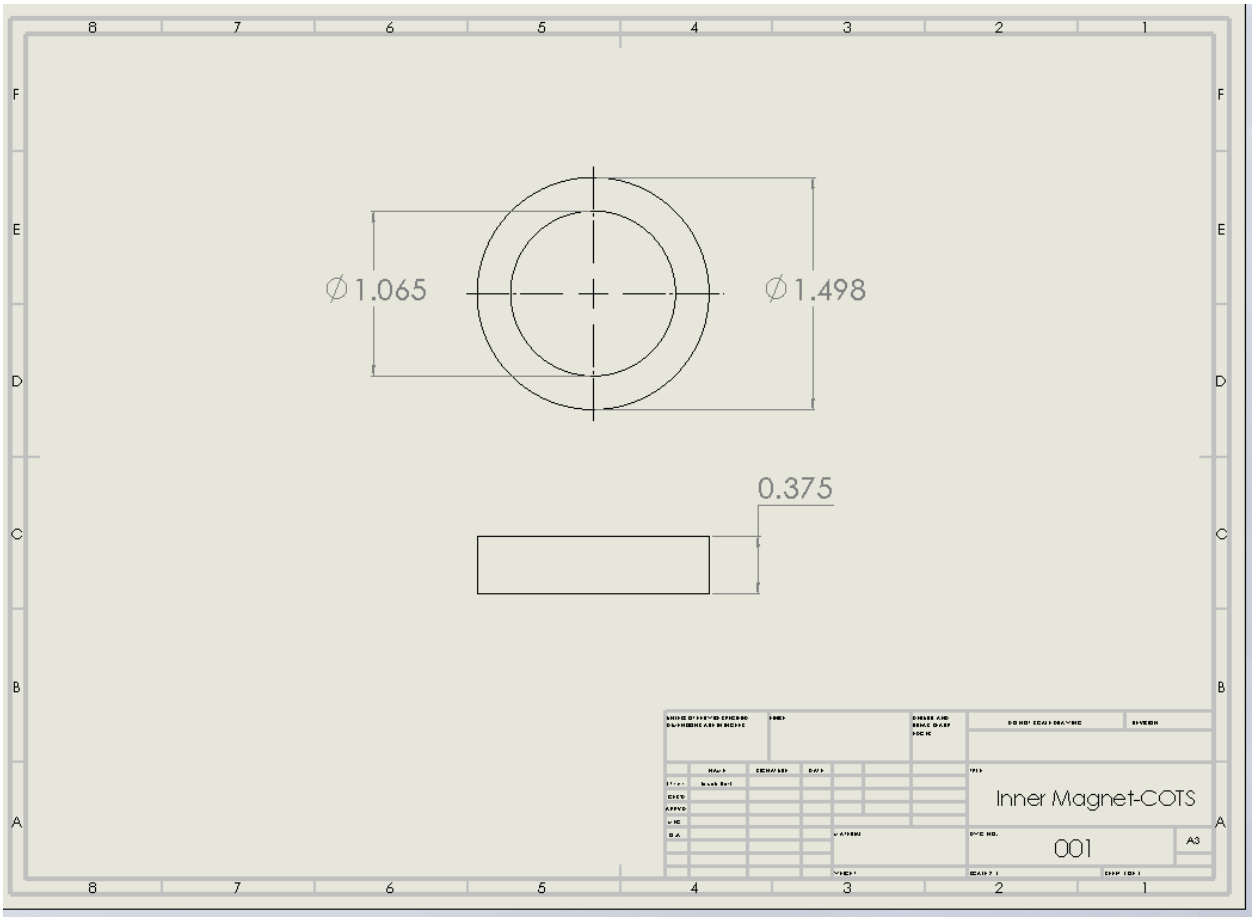

Fig. 14: Inner Neodymium Magnet (Commercial off the Shelf) Schematic

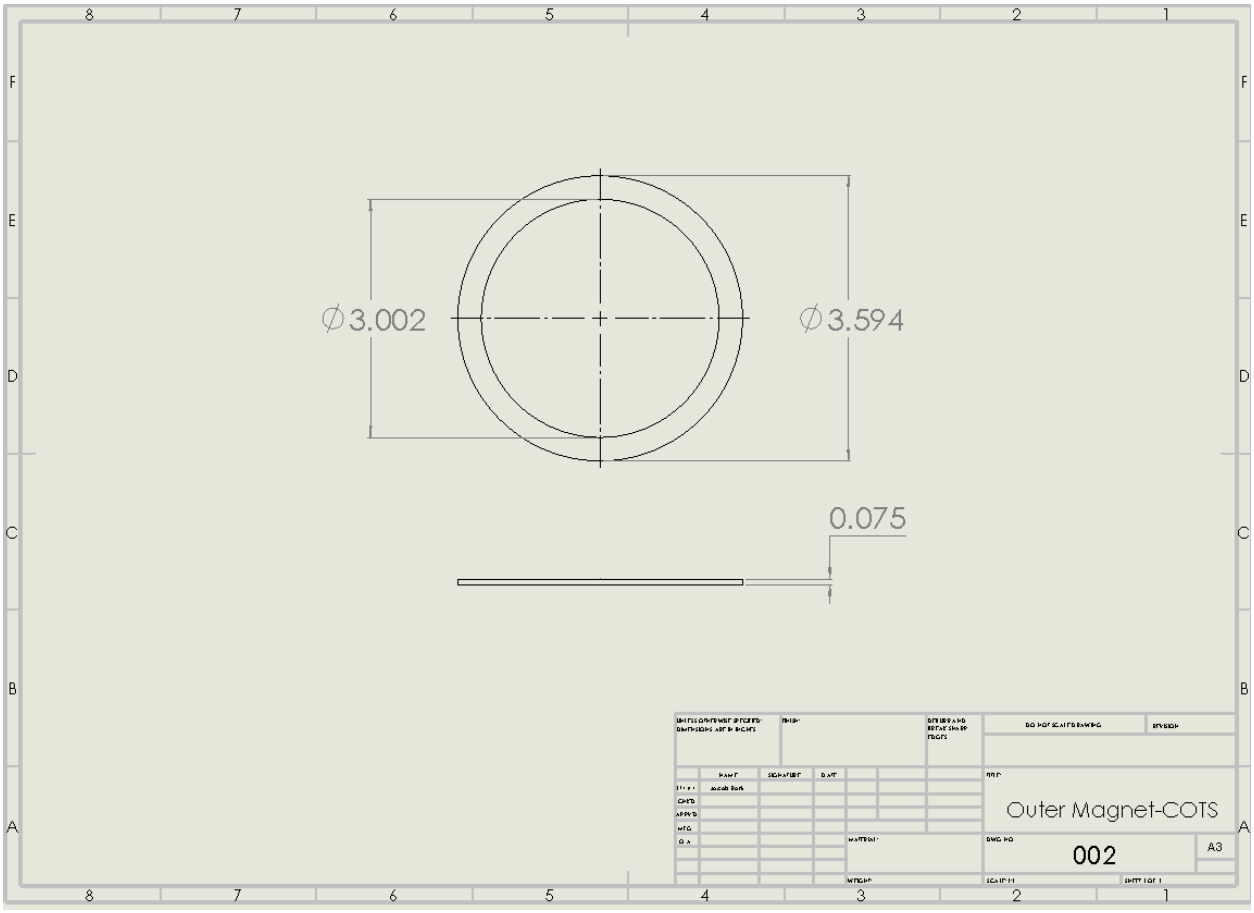

Fig. 15: Outer Neodymium Magnet (Commercial off the Shelf) Schematic

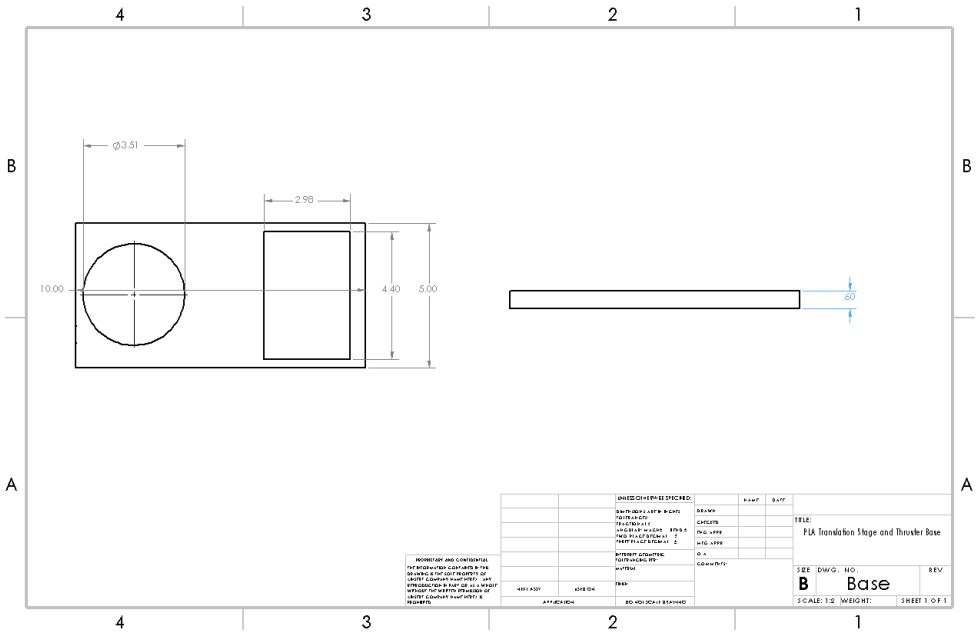

Fig. 16: PLA Translation stage and hall thruster base

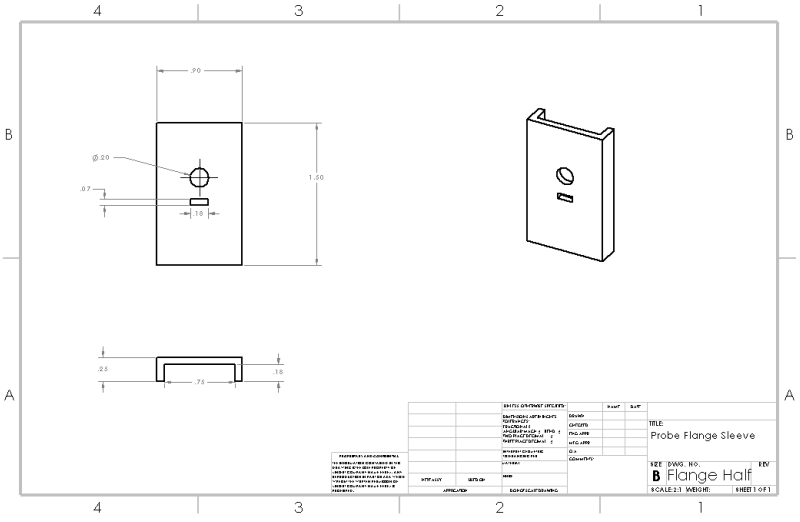

Fig. 17: PLA Probe Flange Sleeve

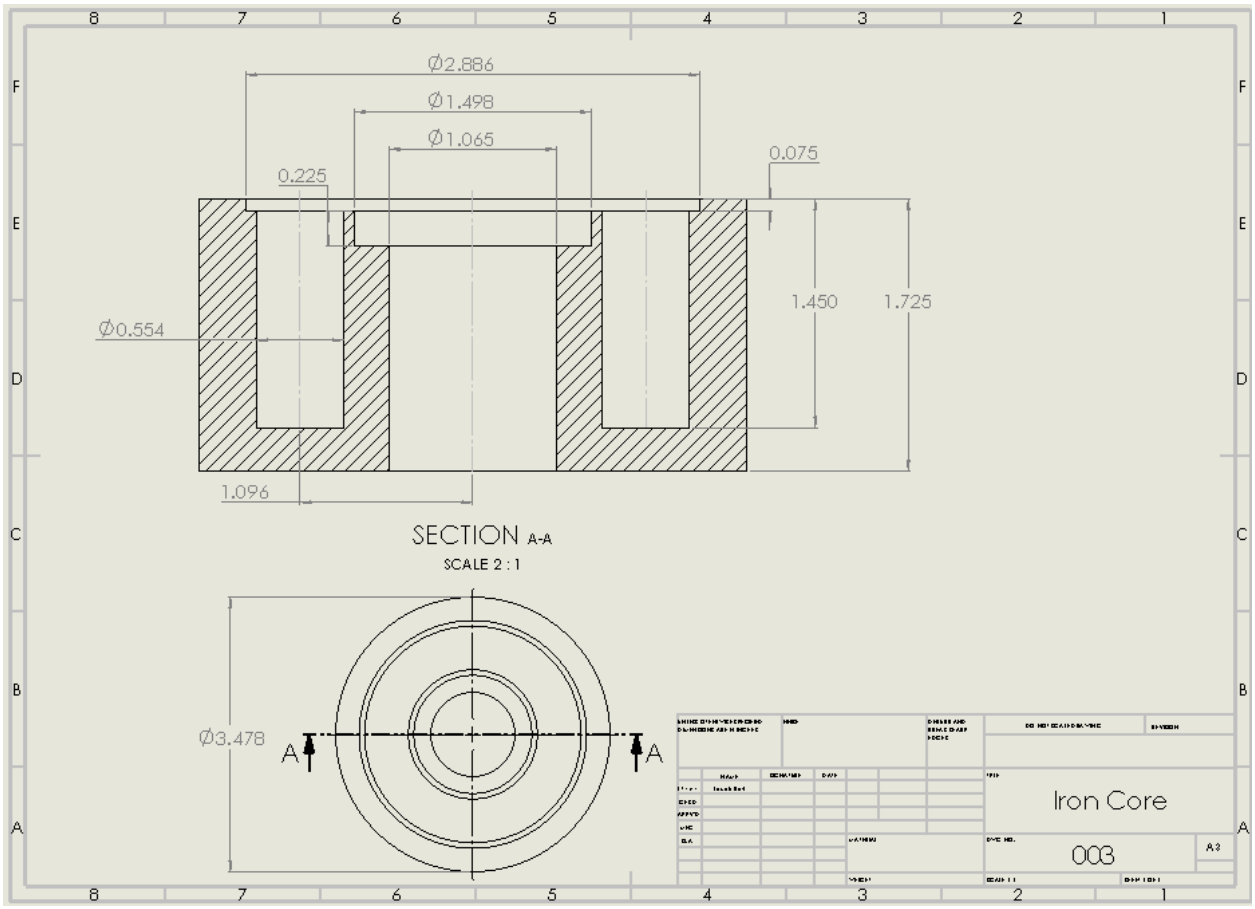

Fig. 18: Machined Iron Core Schematic

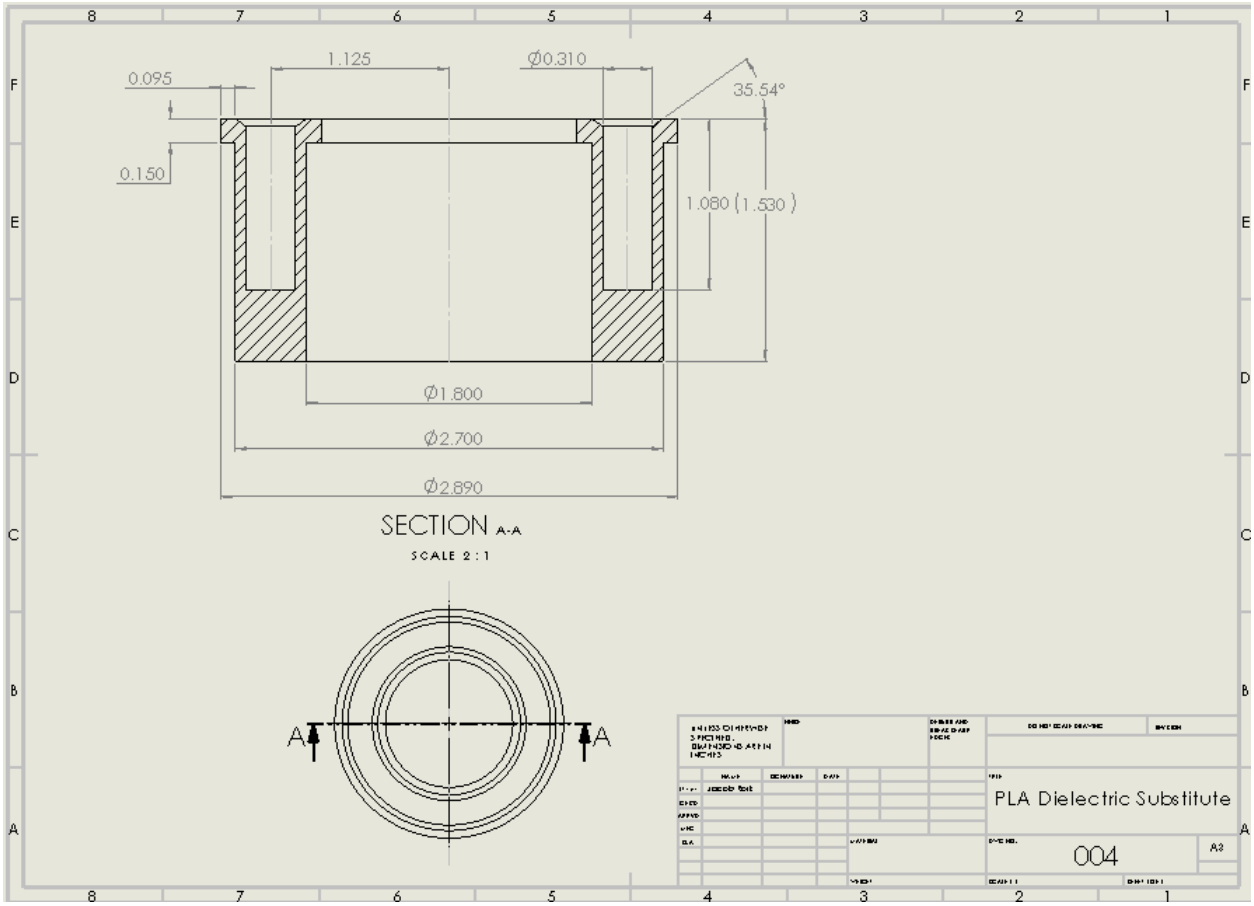

Fig. 19: PLA Dielectric Substitute Schematic

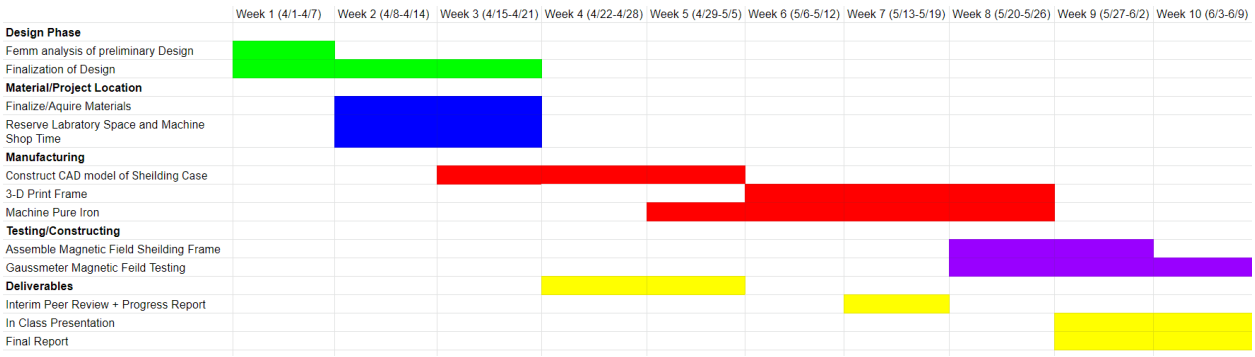

Fig. 20: Final Gantt Chart

Delta Force Final Budget			
Item:	Description:	Quantity:	Cost Per:
Assorted Colors PLA filament	AmazonBasics PLA 3D Printer Filament, 1.75mm, 22 Assorted Colors, 1.25 kg total weight	1	27.78
Inner Magnet	Inner Diameter Neodymium Magnet, 1-1/2" x 1.065" ID x 3/8" Rare Earth Disc Magnet	2	4.24
Outer Magnet	Outer Diameter Neoydimium Magnet, 3-1/2" x 3" ID x .079", R1300 Neoydimium 40	2	35
Machinable Cast Iron	Rounded Cast Iron, 1ft. Long rod, 4" Diameter, code 8909K84, must manually add to cart from list	1	86.56
Gold Amazon Basic PLA filament	AmazonBasics PLA 3D Printer Filament, 1.75mm, Gold, 1.25 kg spool	1	17.09
	Total:		209.91

Fig. 21: Final Project Budget